Inorganic Chemistry

Article

pubs.acs.org/IC

Structural Influence on the Photochromic Response of a Series of Ruthenium Mononitrosyl Complexes

Benoit Cormary,[†,‡] Sonia Ladeira,[†,‡] Kane Jacob,[†,‡] Pascal G. Lacroix,[†,‡] Theo Woike,[§] Dominik Schaniel,[∥] and Isabelle Malfant*[,†,‡]

[†]LCC (Laboratoire de Chimie de Coordination), CNRS, 205 Route de Narbonne, F-31077 Toulouse, France

[‡]UPS, INPT, LCC, Université de Toulouse, F-31062 Toulouse, France

[§]Institut für Strukturphysik, TU Dresden, Zellescher Weg 16, 01062 Dresden, Germany

[∥]CRM2, UMR CNRS 7036, Institut Jean Barriol, Université de Lorraine, BP 70239 Boulevard des Aiguillettes, 54506 Vandoeuvre-les-Nancy, France

Supporting Information

ABSTRACT: In mononitrosyl complexes of transition metals two long-lived metastable states corresponding to linkage isomers of the nitrosyl ligand can be induced by irradiation with appropriate wavelengths. Upon irradiation, the N-bound nitrosyl ligand (ground state, GS) turns into two different conformations: isonitrosyl O bound for the metastable state 1 (MS1) and a side-on nitrosyl conformation for the metastable state 2 (MS2). Structural and spectroscopic investigations on $[RuCl(NO)py_4](PF_6)_2 \cdot 1/2H_2O$ (py = pyridine) reveal a nearly 100% conversion from GS to MS1. In order to identify the factors which lead to this outstanding photochromic response we study in this work the influence of counteranions, trans ligands to the NO and equatorial ligands on the conversion efficiency: $[RuX(NO)py_4]Y_2 \cdot nH_2O$ (X = Cl and Y = PF_6^- (**1**), BF_4^- (**2**), Br^-(**3**), Cl^- (**4**); X = Br and Y = PF_6^- (**5**), BF_4^- (**6**), Br^-(**7**)) and $[RuCl(NO)bpy_2](PF_6)_2$ (**8**), $[RuCl_2(NO)tpy](PF_6)$ (**9**), and $[Ru(H_2O)(NO)bpy_2](PF_6)_3$ (**10**) (bpy = 2,2′-bipyridine; tpy = 2,2′:6′,2″-terpyridine). Structural and infrared spectroscopic investigations show that the shorter the distance between the counterion and the NO ligand the higher the population of the photoinduced metastable linkage isomers. DFT calculations have been performed to confirm the influence of the counterions. Additionally, we found that the lower the donating character of the ligand trans to NO the higher the photoconversion yield.

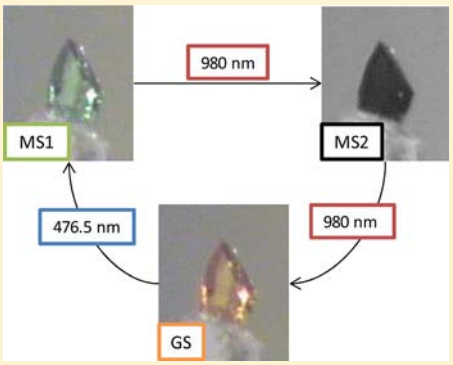

INTRODUCTION

It is of great interest to develop new molecular-based inorganic solids whose physical properties can be controlled by an external perturbation.[1−10] In this context, materials where the photochromic response is based on light-induced linkage isomerism have been largely studied. On one hand, they are of interest for studying fundamental questions like bonding properties in metastable states, and on the other hand, they offer high potential for applications such as data storage and real-time optical applications as well as in the context of photoinduced NO release.[11−14] Especially appealing are photochromic and photorefractive compounds, which allow for reversible switching between well-defined states using different wavelengths and short laser pulses.[15] Since the discovery of long-lived metastable states in the mononitrosyl complex $Na_2[Fe(CN)_5(NO)] \cdot 2H_2O$ (SNP = sodium nitroprusside),[16,17] many complexes containing, e.g., ruthenium, osmium, manganese, iron, nickel, and platinum have been found with similar photophysical behavior.[18−26] Upon irradiation, the conformation of the N-bound nitrosyl ligand (GS, ground state) switches to the isonitrosyl conformation for the metastable state 1 (MS1) and the side-on nitrosyl conformation for the metastable state 2 (MS2).[27−29] A schematic illustration of the photoinduced processes occurring in these salts is shown in Scheme 1. The decay of the metastable states occurs radiationless upon heating, and the enthalpy can be detected by differential scanning calorimetry (DSC).

Scheme 1. Three Possible Structural Configurations for GS, MS1, and MS2 States

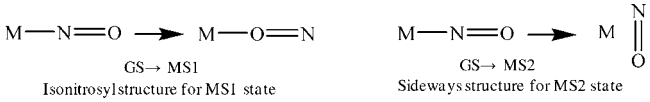

The rotation of the NO ligand observed in the reversible transformation GS → MS2 → MS1 is triggered by the charge transfer transition from metal d orbitals to the nitrosyl π^*(NO) orbital. The necessary conditions for generation of the metastable linkage isomers in ML_5NO-type compounds have been described recently, and a corresponding potential scheme

Received: December 15, 2011
Published: July 3, 2012

   dx.doi.org/10.1021/ic202702r | *Inorg. Chem.* 2012, 51, 7492−7501

has been proposed.[30] First, optical excitation must lead to a change in the bond between the NO group and the central metal atom M, e.g., by a metal-to-ligand charge transfer of type d → π^*(NO), which results in a 2-fold degenerate E state, so that the vibrational deformation mode δ(M−N−O) can drive the system into the linkage configuration on the basis of the Jahn−Teller theorem by lifting the degeneracy.[31,32] The metastable states correspond to minima on the ground state potential surface separated by potential barriers. Second, the excited state potential must possess a minimum close to the saddle point of the ground state surface between GS and MS2 or cross that surface such that the relaxation from the excited state into the metastable minima can occur. For MS2, it was recently shown in SNP crystals that NO rotation is ultrafast (~300 fs) and occurs along a diabatic potential, i.e., there is crossing between the GS and the MS2 potential.[33] We can assume that in all ML_5NO-type compounds formation of MS1 and MS2 occurs in a similar way. The population of the metastable linkage isomers is determined by the ratio of the cross sections for depletion and population at a given wavelength (Scheme 2).

Scheme 2. Potential Scheme for Formation of the Isonitrosyl-Bound Linkage Isomer MS1 in Ruthenium Nitrosyl Complexes

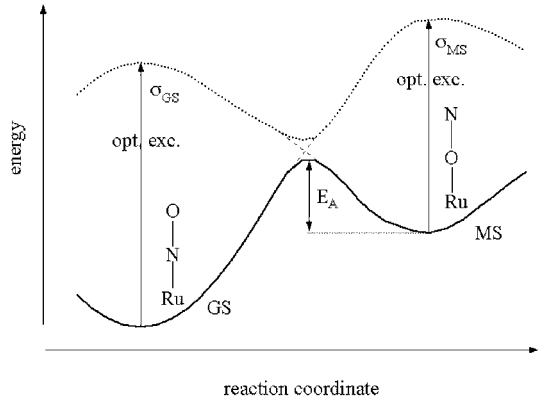

The metastable linkage isomers can be evidenced by the shift of the ν_{NO} stretching vibration, and the population is determined by the decrease of the ν_{NO} band.[34] In the UV−vis spectral range population of MS1 and MS2 leads to a decrease of the absorption bands of the GS and the appearance of new absorption bands characteristic for the metastable states.[35] The energy barriers (activation energy) separating the metastable states from the ground state and the energetic positions of the metastable states can be determined by DSC.[36] Thereby, the stored energy from the metastable states is released as heat to the lattice and detected as enthalpy by DSC.

Recently, we focused on the study of the ruthenium complex $[RuCl(NO)py_4](PF_6)_2 \cdot 1/2H_2O$ (**1**) for which the highest population (92% for MS1 and 48% for MS2 on single crystals) has been observed up to now for this kind of inorganic compounds.[29,34] The previously reported highest populations of about 50% for MS1 were observed in a single crystal of SNP.[17] The almost full photoconversion in **1** allowed for a very precise investigation of the MS1 structural conformation by X-ray diffraction after irradiation, and it could be shown that solid state DFT calculations reproduce the observed linkage isomer structures with high precision concerning bond lengths and angles.[29] The color change as an illustration of the photo-induced processes occurring in this salt is shown in Figure 1, where irradiation with 476.5 nm generates MS1 and subsequent irradiation with 980 nm generates MS2.

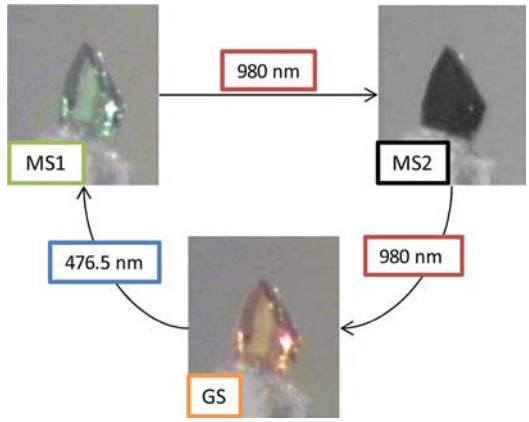

Figure 1. Color change of $[RuCl(NO)py_4](PF_6)_2 \cdot 1/2H_2O$ single crystal at 180 K upon irradiation with laser light of wavelengths 476.5 and 980 nm.

In the present work, we studied the photoswitching behavior of a series of mononitrosyl compounds based on the $[RuCl(NO)py_4]^{2+}$ cation associated with four different counterions PF_6^- (**1**), BF_4^- (**2**), Br^-(**3**), and Cl^- (**4**). Moreover, we changed the trans ligand of NO from Cl to Br and the equatorial ligand from pyridine to 2,2′-bipyridine (bpy) or 2,2′:6′,2″-terpyridine (tpy) ligands, and we studied the metastable states in $[RuBr(NO)py_4]Y_2 \cdot nH_2O$ (Y = PF_6^- (**5**), BF_4^- (**6**), Br^-(**7**)), $[RuCl(NO)bpy_2](PF_6)_2$ (**8**), $[RuCl_2(NO)tpy](PF_6)$ (**9**), and $[Ru(H_2O)(NO)bpy_2](PF_6)_3$ (**10**) (Table 1).

Table 1. Numbering of the Nitrosyl Complexes

complexes	counterions	equatorial ligands	trans ligands
$[RuCl(NO)py_4](PF_6)_2 \cdot 1/2 H_2O$ (**1**)	PF_6	pyridine	Cl
$[RuCl(NO)py_4](BF_4)_2 \cdot 1/2 H_2O$ (**2**)	BF_4	pyridine	Cl
$[RuCl(NO)py_4]Br_2 \cdot 3/2H_2O$ (**3**)	Br	pyridine	Cl
$[RuCl(NO)py_4]Cl_2 \cdot 4H_2O$ (**4**)	Cl	pyridine	Cl
$[RuBr(NO)py_4](PF_6)_2$ (**5**)	PF_6	pyridine	Br
$[RuBr(NO)py_4](BF_4)_2$ (**6**)	BF_4	pyridine	Br
$[RuBr(NO)py_4]Br_2$ (**7**)	Br	pyridine	Br
$[RuCl(NO)bpy_2](PF_6)_2$ (**8**)	PF_6	2,2′-bipyridine	Cl
$[RuCl_2(NO)tpy](PF_6)$ (**9**)	PF_6	2,2′:6′,2″-terpyridine	N_{tpy}
$[Ru(H_2O)(NO)bpy_2](PF_6)_3$ (**10**)	PF_6	2,2′-bipyridine	H_2O

We found that the population of the metastable linkage isomers depends on the distance between the counterion and the NO ligand. The shorter the distance of the counterion to the NO ligand the higher the population is. Further, the lower the donating character of the trans-to-NO ligand the higher the photoconversion yield. This observation allows designing new molecules with optimal photochromic behavior.

dx.doi.org/10.1021/ic202702r | Inorg. Chem. 2012, 51, 7492−7501

Table 2. Selected X-ray Crystallographic Data for 1−5 and 9 at 180 K

	$[RuCl(NO)py_4](PF_6)_2 \cdot 1/2H_2O$, **1**[29]	$[RuCl(NO)py_4](BF_4)_2 \cdot 1/2H_2O$, **2**	$[RuCl(NO)py_4]Br_2 \cdot 3/2H_2O$, **3**	$[RuCl(NO)py_4]Cl_2 \cdot 4H_2O$, **4**	$[RuBr(NO)py_4](PF_6)_2$, **5**	$[RuCl_2(NO)tpy](PF_6)$, **9**
cryst syst	monoclinic	monoclinic	monoclinic	monoclinic	orthorhombic	monoclinic
a (Å)	15.7016 (4)	13.7292(3)	13.8031(3)	20.924(5)	16.814(5)	8.9771(5)
b (Å)	13.4512 (4)	13.3179(2)	12.6530(3)	12.799(6)	12.842(5)	16.2944(8)
c (Å)	26.8147 (7)	18.8043(3)	18.2544(3)	20.172(7)	26.396(5)	12.6972(7)
α (deg)	90	90	90	90	90	90
β (deg)	92.436 (2)	126.324(1)	126.832(1)	150.243(9)	90	95.956(4)
γ (deg)	90	90	90	90	90	90
V (Å^3)	5658.3 (3)	2770.14(9)	2551.78(10)	2681.2(18)	5700.0(3)	1847.28(17)
Z^a	8	4	4	8	8	4
V/Z (Å^3)	707.3	692.5	637.9	335.1	712.4	461.8
space group	$P2_1/c$	$P2_1/c$	$P2_1/c$	$C2/c$	$Pbca$	$P2_1/c$
reflns collected/ unique	41 039/12 319	31 528/8131	56 567/5175	12 764/2586	24 504/5224	18 897/5620
final R indices [$I > 2\sigma(I)$]	R_1 = 0.0277	R_1 = 0.0645	R_1 = 0.0447	R_1 = 0.0251	R_1 = 0.0288	R_1 = 0.0253
	wR_2 = 0.063	wR_2 = 0.2009	wR_2 = 0.1236	wR_2 = 0.0622	wR_2 = 0.0612	wR_2 = 0.0547
R indices (all data)	R_1 = 0.043	R_1 = 0.1018	R_1 = 0.0523	R_1 = 0.0278	R_1 = 0.0468	R_1 = 0.0453
	wR_2 = 0.0695	wR_2 = 0.2427	wR_2 = 0.1312	wR_2 = 0.0641	wR_2 = 0.0676	wR_2 = 0.0589

[a]Number of formula units in the unit cell.

EXPERIMENTAL SECTION

Reagents and General Procedure. The following chemicals and reagents were used as received: $RuCl_3 \cdot xH_2O$ (Aldrich), NBu_4Br, NBu_4Cl, and $NBu_4(BF_4)$ (Aldrich). Solvents were used without purification (CH_3CN from SDS Co. (HPLC grade), pyridine from Aldrich (99%)). The photochromic complexes $[RuCl(NO)py_4](PF_6)_2 \cdot 1/2H_2O$ (**1**) and $[RuBr(NO)py_4](PF_6)_2$ (**5**) were prepared following previously reported procedures.[34] Complexes $[RuCl(NO)bpy_2](PF_6)_2$ (**8**), $[Ru(H_2O)(NO)bpy_2](PF_6)_3$ (**10**), and $[RuCl_2(NO)tpy](PF_6)$ (**9**) were already described by Nagao et al.,[37a] Meyer et al.,[37b] and Ferlay et al.[38]

Synthesis. A 60 mg (0.08 mmol for **1**, 0.09 mmol for **5**) amount of complex was dissolved in a minimum amount of acetonitrile. A 250 mg amount of the appropriate NBu_4Y salt (Y = Cl^- (**4**) (0.78 mmol), Br^- (**3** and **7**) (0.69 mmol), and BF_4^- (**2** and **6**) (0.67 mmol)) dissolved in 5 mL of acetonitrile was added dropwise to the previous solution. An orange powder appears after a few minutes of stirring. The product was washed with a minimum amount of acetonitrile. For **1**: yield 92%. Anal. Calcd: C, 30.72; H, 2.71; N, 8.96. Found: C, 30.79; H, 2.47; N, 8.94. For **2**: yield 89%. Anal. Calcd: C, 36.09; H, 3.18; N, 10.52. Found: C, 35.91; H, 3.37; N, 10.60. For **3**: yield 95%. Anal. Calcd: C, 35.87; H, 3.46; N, 10.46. Found: C, 35.74; H, 3.68; N, 10.35. For **4**: yield 96%. Anal. Calcd: C, 38.38; H, 4.51; N, 11.19. Found: C, 38.21; H, 4.17; N, 11.10. For **5**: yield 92%. Anal. Calcd: C, 29.39; H, 2.47; N, 8.57. Found: C, 29.45; H, 2.33; N, 8.71. For **6**: yield 96%. Anal. Calcd: C, 34.27; H, 2.88; N, 9.99. Found: C, 34.32; H, 2.81; N, 9.90. For **7**: yield 93%. Anal. Calcd: C, 34.96; H, 2.93; N, 10.19. Found: C, 34.78; H, 3.00; N, 10.04. For **8**: yield 91%. Anal. Calcd: C, 31.24; H, 2.10; N, 9.11. Found: C, 31.13; H, 2.09; N, 9.34. For **9**: yield 94%. Anal. Calcd: C, 31.05; H, 1.91; N, 9.66. Found: C, 31.27; H, 1.68; N, 9.41. For **10**: yield 90%. Anal. Calcd: C, 26.80; H, 2.02; N, 7.81. Found: C, 26.56; H, 2.13; N, 8.01.

FT-IR spectra: for **1** $\nu_{NO} \approx 1911$ cm^{-1} (m), for **2** $\nu_{NO} \approx 1920$ cm^{-1} (m), for **3** $\nu_{NO} \approx 1911$ cm^{-1} (m), for **4** $\nu_{NO} \approx 1917$ cm^{-1} (m), for **5** $\nu_{NO} \approx 1909$ cm^{-1} (m), for **6** $\nu_{NO} \approx 1919$ cm^{-1} (m), for **7** $\nu_{NO} \approx 1913$ cm^{-1} (m); absence of PF_6^- significant signal $\nu_{PF} = 832$ cm^{-1}. For **8** $\nu_{NO} \approx 1928$ cm^{-1}(m), for **9** ν_{NO} is at 1896, 1914, and 1925 cm^{-1}; $\nu_{PF} = 832$ cm^{-1} (s) for **8**, **9**, and **10**. For **10** $\nu_{NO} \approx 1940$ cm^{-1} (m).

Instrumentation. Elemental analyses were performed on a Perkin Elmer 2400-II analyzer. IR spectra were recorded in transmission geometry on a Perkin Elmer GX2000 and a Nicolet 5700 FT-IR spectrophotometer operating from 400 to 4000 cm^{-1}. The fine powder of the samples was mixed with KBr and pressed to a pellet. Infrared measurements upon irradiation were performed on the Nicolet spectrophotometer with a resolution of 2 cm^{-1}. The pellet was mounted on a copper coldfinger cooled to 100 K in a home-built cryostat equipped with CsI windows. Irradiation was performed using monochromatic light of an Ar^+ laser (λ = 476.5 nm), a diode laser (980 nm), and a Nd:YAG laser (λ = 1064 nm) up to saturation.

X-ray Diffraction. Single crystals suitable for X-ray crystallographic analyses were obtained by slow evaporation of an acetonitrile/water mixture. Crystal data have been collected on an Oxford Diffraction XCALIBUR diffractometer, equipped with an Oxford Cryosystems cooler device, using graphite-monochromated Mo Kα radiation (λ = 0.71073 Å). Structures were solved by direct methods and refined by least-squares procedures on F^2 with the aid of the program SHELXL-97.[39] All non-hydrogen atoms were anisotropically refined. Hydrogen atoms were fixed by a riding model. Crystallographic figures have been generated by ORTEP, with 30% probability displacement ellipsoids for non-hydrogen atoms.[39]

DFT Calculations. Gas-phase geometries for $[RuCl(NO)py_4]^{2+}$ and $[RuCl(ON)py_4]^{2+}$ cations were fully optimized using the Gaussian-09 program package[40] within the framework of the DFT at the B3LYP/6-31G*/LANL2DZ(Ru) level.[41−43] The starting metrical parameters for the calculations were taken from the present crystal structures. No symmetry was imposed in the computations. However, C_4 symmetry is observed in the final geometries within a tolerance of 0.002 Å for $[RuCl(NO)py_4]^{2+}$ and 0.001 Å for $[RuCl(ON)py_4]^{2+}$.

To check the effect of the environment on the relative stability of both Ru−NO and Ru−ON isomers, calculations were performed on $[RuCl(NO)py_4](PF_6)_2$ and $[RuCl(ON)py_4](PF_6)_2$.

Results are consistent with the X-ray data (in particular, it is observed that the Ru−N−O and Ru−O−N fragments are linear). Moreover, frequency calculations indicate a lowering of the NO vibration frequency in the gas phase from 1975 to 1927 cm^{-1} on passing from Ru−NO to Ru−ON, in qualitative agreement with the IR data.

RESULTS AND DISCUSSION

Molecular Structure. Crystal structures of **1**−**5** and **9** were investigated. Crystal data for compounds **1**−**5** and **9** are given in Table 2. Compounds **1**−**3** and **9** crystallize in the same monoclinic $P2_1/c$ space group, whereas analogues **4** and **5** have two different space groups, monoclinic $C2/c$ for **4** and orthorhombic $Pbca$ for **5**.

Complexes **1** and **4** show two ruthenium cations and one-half a ruthenium molecule, respectively, in the asymmetric unit,

dx.doi.org/10.1021/ic202702r | Inorg. Chem. 2012, 51, 7492−7501

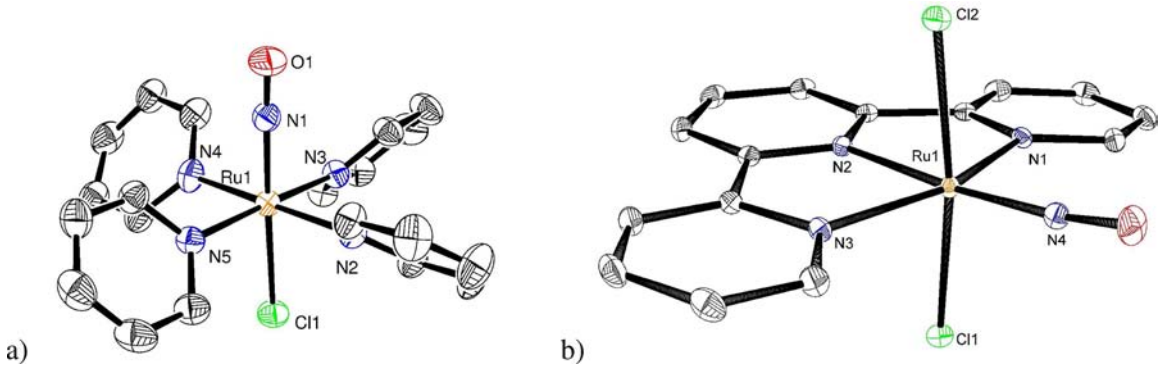

Figure 2. View of complexes **2** $[RuCl(NO)py_4]^{2+}$ (a) and **9** $[RuCl_2(NO)tpy]^{+}$ (b) at 180 K.

Table 3. MS1 Population Linked to Crystallographic Data and/or Counterion Volume for Complexes 1−7

complexes	space group	Ru−N−O angle (deg)	P_{MS1}	counterion	counterion vol. (Å^3)
$[RuCl(NO)py_4](PF_6)_2\cdot 1/2H_2O$ (**1**)	$P2_1/c$	178.3(2)/172.3(2)	76%	PF_6	120.02
$[RuCl(NO)py_4](BF_4)_2\cdot 1/2H_2O$ (**2**)	$P2_1/c$	177.6(5)	45%	BF_4	89.99
$[RuCl(NO)py_4]Br_2\cdot 3/2H_2O$ (**3**)	$P2_1/c$	176.0(4)	17%	Br	26.52
$[RuCl(NO)py_4]Cl_2\cdot 4H_2O$ (**4**)	$C2/c$	180.0(1)	11%	Cl	22.45
$[RuBr(NO)py_4](PF_6)_2$ (**5**)	$Pbca$	175.4(3)	46%	PF_6	120.02
$[RuBr(NO)py_4](BF_4)_2$ (**6**)			28%	BF_4	89.99
$[RuBr(NO)py_4]Br_2$ (**7**)			5%	Br	26.52

Table 4. Angles in 1−5 and 9 in the Ground State from XRD Refinement

complexes	Ru−N−O angle (deg)	N_{ring}−Ru−N_{ring} angle (deg)	N_{ring}−Ru−X (X = Cl or Br) angle (deg)
$[RuCl(NO)py_4](PF_6)_2\cdot 1/2H_2O$ (**1**)	178.3(2)/172.3(2)	89.96(7)	88.18(5)
$[RuCl(NO)py_4](BF_4)_2\cdot 1/2H_2O$ (**2**)	177.6(5)	91.67(16)−90.93(17)	87.16(12)−89.17(12)
$[RuCl(NO)py_4]Br_2\cdot 3/2H_2O$ (**3**)	176.0(4)	86.67(14)−91.78(14)	86.71(10)−90.31(11)
$[RuCl(NO)py_4]Cl_2\cdot 4H_2O$ (**4**)	180.0(1)	88.8(4)−91.3(4)	87.0(3)−91.4(3)
$[RuBr(NO)py_4](PF_6)_2$ (**5**)	175.4(3)	88.91(11)−91.04(10)	87.71(8)−89.38(8)
$[RuCl_2(NO)tpy](PF_6)$ (**9**)	173.2(2)	78.80(6)	88.06(5)

Table 5. Interatomic Distances in Complexes 1−5 and 9 from XRD Refinement

complexes	Ru−N_{NO} (Å)	N−O (Å)	Ru−X (X = Cl or Br) (Å)	Ru−N_{ring} (Å)
$[RuCl(NO)py_4](PF_6)_2\cdot 1/2H_2O$ (**1**)	1.752(2)/1.759(2)	1.148(2)/1.142(2)	2.325(1)/2.323(1)	2.113(2)/2.110(2)
$[RuCl(NO)py_4](BF_4)_2\cdot 1/2H_2O$ (**2**)	1.757(4)	1.120(6)	2.317(2)	2.104(4)
$[RuCl(NO)py_4]Br_2\cdot 3/2H_2O$ (**3**)	1.753(4)	1.126(5)	2.335(1)	2.109(4)
$[RuCl(NO)py_4]Cl_2\cdot 4H_2O$ (**4**)	1.756(3)	1.117(4)	2.329(1)	2.104(2)
$[RuBr(NO)py_4](PF_6)_2$ (**5**)	1.752(3)	1.131(3)	2.465(1)	2.109(3)
$[RuCl_2(NO)tpy](PF_6)$ (**9**)	1.759(2)	1.131(2)	2.337(1)/2.363(1)	2.073(2)

whereas the other compounds have just one ruthenium cation. Except for **5** and **9**, all systems contain crystal water in the asymmetric unit. The volume of the unit cell V normalized to the number of molecules in the unit cell Z decreases from compound **1** to **4** so that the packing density increases.

For mononitrosyl $\{M-NO\}^6$ photochromic complexes such as $[Fe(CN)_5NO]^{2-}$, $[RuCl_5NO]^{2-}$, or $[RuNO(NH_3)_5]^{3+}$, the M−NO group is linear in the ground state. Similarly, the conformation of the nitrosyl ligand in **1**−**5** and **9** is quasilinear (Figure 2). The different values for the M−N−O angle reported in Tables 3 and 4 range from 180.0°(1) to 172.3°(2).

The largest N−O bond lengths (1.148(2) and 1.142(2) Å) and equatorial Ru−N_{ring} distances (2.113(2) and 2.110(2) Å) are found in **1** where the counteranion is the hexafluorophosphate ion.

In **1**−**5**, the Ru−N_{ring} distances are very close to 2.10 Å. Moreover, the pyridine ligands are not located in the same plane. Each pyridine ring is quasiperpendicular to its trans analogue with an angle around 90° (Table 4). Interatomic distances are comparable for the six complexes. The biggest variation is observed for Ru−X (X = Cl or Br) going from 2.317(2) Å in **2** to 2.465(1) Å in **5** in agreement with the more voluminous radius of the bromide versus the chloride ligand. This feature does not affect the Ru−N_{NO} bond length, which is between 1.752(2) and 1.759(2) Å (Table 5).

In $[RuCl_2(NO)tpy](PF_6)$ (**9**), the ruthenium(II) ion is located at the center of a distorted octahedron with the chloro ligands in a mutual trans position: the Cl−Ru−Cl angle is 171.9(2)°. The terpyridine ligand is planar, and the NO ligand is not coplanar with it: the nitrosyl forms an angle of 175.3(1)° with the central nitrogen atom of the terpyridine. The nitrosyl ligand is quasilinear (Ru−N−O = 173.2(2)°). The Ru−N_{NO} bond distances are similar to those in $[RuCl(NO)py_4]$-

dx.doi.org/10.1021/ic202702r | Inorg. Chem. 2012, 51, 7492−7501

Table 6. Intermolecular contacts (in Angstroms), Shorter than the Sum of the van der Waals Radii, Observed Between the $[RuX(NO)py_4]^{2+}$ Complex, Counteranion, and Crystallization Water Molecules in 1−5[a]

d_{inter} (Å)	Σ_{Rvdw} (Å)	PF_6^-, **1**	BF_4^-, **2**	Br^-, **3**	Cl^-, **4**	PF_6^-, **5**
O_{NO}−F	3.00	2.906(3), 2.913(3) 2.932(2), 2.900(2), 2.802(2)	2.725(12)			2.680(13), 2.696(14)
O_{NO}−O_{H2O}	2.80				2.571(4)	
(*trans*-Cl)−H (H_2O)	3.01	2.390(20)		2.60(30)		

[a] $[RuCl(NO)py_4]Y_2 \cdot nH_2O$ (Y = PF_6 (**1**), BF_4 (**2**), Br (**3**), Cl (**4**)) and $[RuBr(NO)py_4](PF_6)_2$ (**5**).

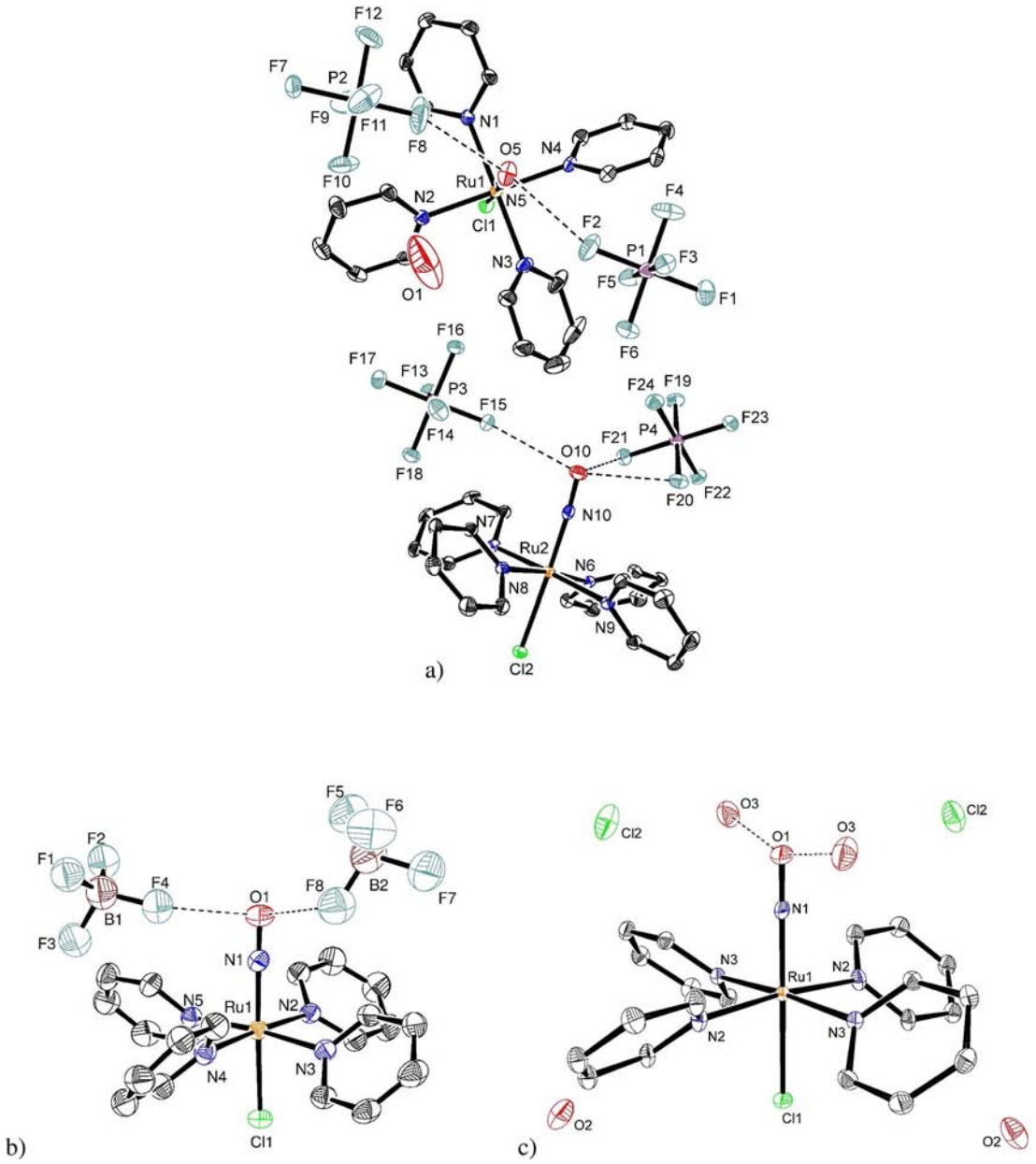

Figure 3. Intermolecular contacts between the oxygen atom of the nitrosyl ligand and the closest neighbors in **1** (a), **2** (b), and **4** (c).

$(PF_6)_2 \cdot 1/2H_2O$ (**1**), while the N−O distance of 1.131(2) Å is slightly shorter than those observed in **1** (Figure 2).

The tetrahedral counteranion BF_4^- shows a small distortion with angles around 109.5° ± 5°. In complex **5**, one of the PF_6^- anions is highly disordered probably due to the vicinity of the pyridine ligand while the second one is almost perfectly octahedral (F−P−F = 90° ± 1°) as in complexes **1** and **9**.

There are numerous intermolecular contacts between the oxygen atom from the nitrosyl ligand and atoms from the counteranions (Table 6). These contacts, which are defined as a distance lower than the sum of van der Waals radii, attest to intermolecular interactions between the cation, particularly to the nitrosyl ligand. Therefore, they may change the photochromic response. Contacts between the trans-ligand Cl and crystal water molecules are observed in **1** and **3**. In the case of $[RuCl(NO)py_4](PF_6)_2 \cdot 1/2H_2O$ (**1**) we observed four intermolecular contacts between the fluorine and the oxygen atoms. The number of intermolecular interactions on oxygen atoms is

dx.doi.org/10.1021/ic202702r | *Inorg. Chem.* 2012, 51, 7492−7501

lower in **2** with BF_4^- counterions. When the counteranion is Cl^- or Br^-, no contact was observed between the oxygen atom of the NO ligand and the anion (Figure 3).

IR Spectra of GS and upon Irradiation. The reversible structural change can be evidenced by infrared spectroscopy upon irradiation at low temperature (100 K), where the lifetime of the NO linkage isomers is longer than 10^9 s. Indeed, the existence of metastable states is associated with the nitrosyl ligand interconversion which is easily observable by the shift of the ν_{NO} vibration frequency to lower frequencies. The GS peak area ratio before and after irradiation in the absorbance spectra allows evaluating the population of the metastable states MS1 and MS2. In previous work[34] on a powder sample of **1**, the population was found to be 76% for the isonitrosyl conformation (MS1) and 56% for the side-on conformation (MS2). Furthermore infrared spectroscopy allows identifying subtle influences of cations or anions and crystal water by small shifts or amplitude variations in the corresponding vibrational bands upon photoexcitation. We consider exemplarily the results obtained on compounds **1** and **2** as they exhibit the highest population. The results on the other compounds are given in tabular form, and corresponding spectra can be found in the Supporting Information (Figures S1 and S2). Infrared spectra collected at 100 K for GS of **1** and **2** are reported in Figure 4. These allow for assignment of the vibrational bands and especially to identify the NO related vibrations at 1906/1914/1919 (**1**) and 1896/1914/1921/1929/1942 cm^{-1} (**2**) for the ν(NO) stretching vibration, at 614 (**1**) and 609 cm^{-1} (**2**) for the δ(Ru−N−O) deformational mode, and at 606 (**1**) and 603 cm^{-1} (**2**) for the ν(Ru−NO) stretching vibration. The splitting of the ν(NO) bands is due to different crystalline environments for different positions of the cation and crystal water in the crystallographic unit cell. Furthermore, the ν(Ru−Cl) stretching vibrations of the trans-to-NO ligand are visible at 458/454 and 452 cm^{-1} for **1** and **2**, respectively. They can be unambiguously identified due to the decrease of the bands after irradiation. Vibrational bands of the anions are found at 832/837/843/851 cm^{-1} for PF_6^- (**1**) and in the range 1000−1200 cm^{-1} as well as at 521/534 cm^{-1} for BF_4^- (**2**). The strong anionic vibrational bands provide a very sensitive signature for the purity of the other compounds, where they have been replaced by Br^- (**3**) and Cl^- (**4**). The vibrational bands originating from the pyridine rings are found in the range 650−1650 cm^{-1} and can be separated from the anionic vibrational bands by comparison of **1** and **2**.

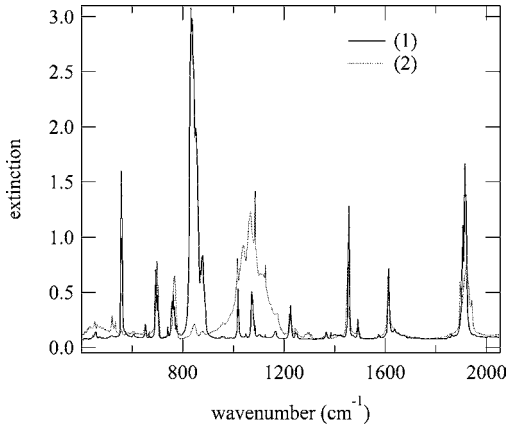

Figure 4. Infrared spectra of GS in **1** and **2** at 100 K.

Figure 5 shows the vibrational spectra of **2** in the range 1500−2200 and 400−650 cm^{-1} after irradiation. The MS1 state is generated by irradiation with light at 476.5 nm up to saturation, which corresponds to an exposure Q of about 300 $J{\cdot}cm^{-2}$. The area of the ν(NO) GS vibrational bands decreases by 45%, and a new band at 1780 cm^{-1} appears however without the strong splitting compared to GS. State MS2 is generated in a two-step process, generating at first MS1 with λ = 476.5 nm up to saturation and subsequently irradiating with infrared light at λ = 1064 nm (Q = 200 $J{\cdot}cm^{-2}$). This leads to a decrease of the MS1 band (1780 cm^{-1}) together with a small increase of GS and the appearance of MS2 at around 1625 cm^{-1}. Due to the overlap of MS2 with the $\delta(H_2O)$ vibration at 1611 cm^{-1} the precise position of MS2 was determined from the difference spectrum of GS−MS2. Again, the strong splitting of the ν(NO) GS vibration is absent in MS2. The population of MS2 is 25%. The downshift of about 140 cm^{-1} for MS1 and about 300 cm^{-1} for MS2 observed for compounds **1**−**7** is comparable to the downshift detected in other mononitrosyl photochromic compounds.[34,44−49]

In the low-energy range 400−650 cm^{-1} the changes upon irradiation allow for identification of the δ(Ru−N−O) deformational mode at 603/610 cm^{-1} which diminishes while vibrational bands of MS1 and MS2 appear at 483 and 567 cm^{-1}. Furthermore, one observes the disappearance of the ν(Ru−Cl) stretching vibration of the trans ligand at 452 cm^{-1} in MS1, while for MS2 it reappears at 452 cm^{-1}. Given the fact that the Ru−Cl distance shortens from 2.32 Å in GS to 2.28 Å in MS1[29] we could expect a hardening of this vibration, and so the band at 483 cm^{-1} might correspond to the Ru−Cl stretching vibration in MS1.

Due to the fact that the ground state ν(NO) band is isolated and proportional to the concentration of unchanged molecules, its area can be accurately determined before and after irradiation in order to calculate the amount of transferred molecules for all investigated compounds. The correspondingly determined populations of the metastable states and the downshifts are reported in Table 7.

In the case of **3** and **4**, where the counteranion PF_6^- is substituted by a halide anion, the metastable states population decreases drastically. Substitution of hexafluorophosphate for the tetrafluoroborate anion leads to a decrease of the population from 76% for **1** to 45% for **2**. The same behavior is observed between **5** and **6**, where the population of MS1 decreases from 46% to 28%. In the infrared spectra this behavior is reflected in the bands of the PF_6^- and BF_4^- anions (Figure 6). While in **1** a clear change of the amplitude of the PF_6^- bands is observed, the vibrational bands of the BF_4^- anions in **2** are only slightly affected upon irradiation. In **1** the central PF_6^- band at 832 cm^{-1} decreases in MS1 and increases in MS2.

The MS1 states were detected in **8** and **9** after irradiation. The area of the NO band for the ground state decreases in both cases. The GS → MS1 conversion is 15% for **8** with bipyridine ligands and 8% for **9** with the terpyridine ligand. The new MS1 signals are weak but clearly visible at 1810 and 1789 cm^{-1} for **8** and **9**, respectively. Changing the trans ligand in the bipyridine compounds from Cl in **8** to H_2O in **10** has a positive effect on the population of MS1 as it increases from 15% in **8** to 19% in **10**.

Counteranions and Crystal Water. The observations evidence the influence of the counteranion on the photochromic response. The drastic variation of the metastable state

dx.doi.org/10.1021/ic202702r | Inorg. Chem. 2012, 51, 7492−7501

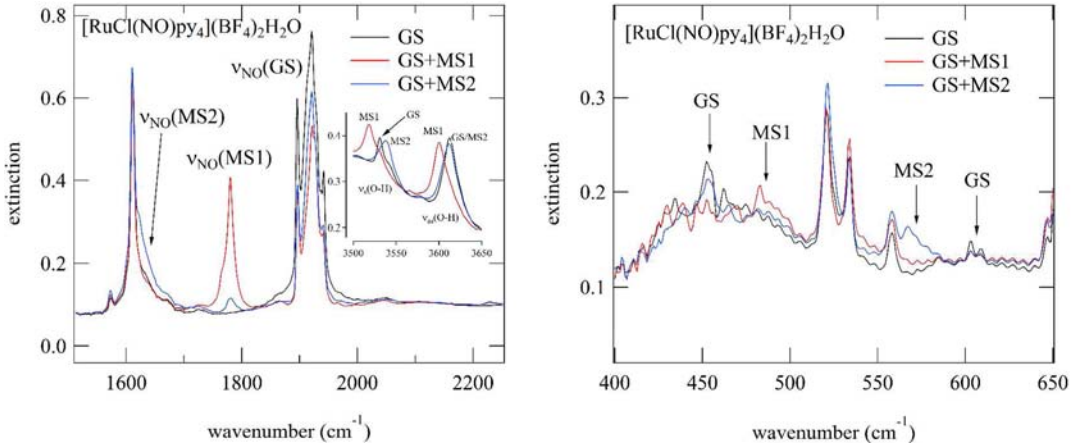

Figure 5. Infrared spectra of GS, MS1, and MS2 in **2** at 100 K: 1500−2250 cm^{-1} (inset 3500−3650 cm^{-1}) range (left) and 400−650 cm^{-1} range (right).

Table 7. ν_{NO} Downshift and Populations of the MS1 and MS2 Metastable State in $[RuX(NO)py_4]^{2+}$

compounds	ν_{GS} (cm^{-1})	ν_{MS1} (cm^{-1})	ν_{NO} downshift (cm^{-1})	P_{MS1} (%)	P_{MS2} (%)
$[RuCl(NO)py_4](PF_6)_2 \cdot 1/2H_2O$ (**1**)	1911	1777	134	76	56
$[RuCl(NO)py_4](BF_4)_2 \cdot 1/2H_2O$ (**2**)	1920	1781	139	45	25
$[RuCl(NO)py_4]Br_2 \cdot 3/2H_2O$ (**3**)	1911	1768	143	17	13
$[RuCl(NO)py_4]Cl_2 \cdot 4H_2O$ (**4**)	1917	1775	142	11	10
$[RuBr(NO)py_4](PF_6)_2$ (**5**)	1909	1764	145	46	18
$[RuBr(NO)py_4](BF_4)_2$ (**6**)	1919	1773	146	28	
$[RuBr(NO)py_4]Br_2$ (**7**)	1913	1770	143	5	

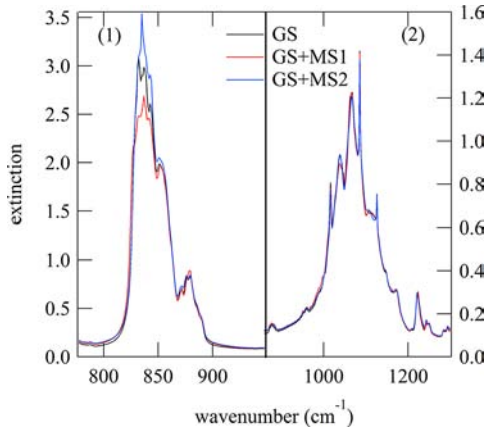

Figure 6. Infrared spectra of GS, MS1, and MS2 at 100 K: in **1** P−F region (left), in **2** B−F region (right).

populations in complexes **1**−**3** (76% for **1**, 45% for **2**, and 17% for **3** for MS1; 56% for **1**, 25% for **2**, and 13% for **3** for MS2), which crystallize in the same space group, indicates that the symmetry relations have no direct influence on the photocommutation (Table 3 and 7).

Note that the population for MS1 decreases regularly when the counteranion is less voluminous, from 76% for **1** to 11% for **4** and from 46% to 5% for **5** and **7**, respectively (Table 3, Figure 3). Moreover, when the anion is bigger, the structural investigations confirm that the intermolecular contacts between the ruthenium cation and the counteranion increase (Table 6). The short contacts observed between the nitrosyl ligand and the counteranion in the case of **1** and **2** correspond to the highest light-induced populations. Therefore, we can assume that they facilitate rotation of the NO ligand and in consequence the population.

Short contacts between the ruthenium cation and the crystal water are observed via the oxygen or hydrogen atoms of H_2O in **1** and **4**, but they have no visible influence on the photoconversion rate as both low and high populations are observed under these conditions. Several intermolecular contacts are present between equatorial ligands and water molecules (distance between 1.7 and 2.4 Å). In **2** the population of MS1 induces a shift of the symmetric ν_s(O−H) and asymmetric ν_{as}(O−H) vibrations to lower wave numbers from ν_s(O−H) = 3531 (GS) to 3519 cm^{-1} (MS1) and from ν_{as}(O−H) = 3613 (GS) to 3600 cm^{-1}. For MS2, however, the wavenumber increases to ν_s(O−H) = 3538 cm^{-1} but ν_{as}(O−H) = 3613 cm^{-1} is the same as in GS. In the isonitrosyl configuration the N···H hydrogen bond is much weaker compared to O···H hydrogen bonds in GS, and so the vibrations shift to lower wave numbers. In MS2 the N−O ligand rotates by 90°, and if the oxygen is slightly approaching the hydrogen the bonds become stronger, which affects ν_s(O−H) but not ν_{as}(O−H).

On the other hand, the presence of fluoro atoms in the PF_6^- and BF_4^- counterion leads to an important increase of the metastable state population (compounds **1**, **2**, **5**, and **6**) in comparison to the other systems (compounds **3**, **4**, and **7**) with the Cl^- or Br^- counterions, in which the populations are not as high.[50] In conclusion, the photochromic response is enhanced by the presence of short contacts between the ruthenium cation and the neighboring atoms especially with fluorine ones.

DFT Calculations. Computed geometries for the free cations (without counteranion) are first compared to the X-ray data in Table 8 in order to evaluate the reliability of the DFT approach for the present complexes. In both GS and MS1 a

dx.doi.org/10.1021/ic202702r | Inorg. Chem. 2012, 51, 7492−7501

Table 8. DFT-Computed Bond Lengths in the Coordination Sphere of $[RuCl(NO)py_4](PF_6)_2$ and $[RuCl(ON)py_4](PF_6)_2$ Compared to X-ray Data for 1[29]

complex	distances (Å)	DFT	X-ray data
$[RuCl(NO)py_4]^{2+}$	$Ru-N_{NO}$	1.779(1.770)[a]	1.752(2)/1.759(2)
	$Ru-N_{py}$	2.149(2.159)	2.113(2)/2.110(2)
	Ru−Cl	2.380(2.336)	2.325(1)/2.323(1)
	N−O	1.136(1.149)	1.148(2)/1.142(2)
$[RuCl(ON)py_4]^{2+}$	$Ru-O_{ON}$	1.925(1.887)	1.862(2)/1.863(2)
	$Ru-N_{py}$	2.145(2.152)	2.095(2)/2.096(2)
	Ru−Cl	2.343(2.301)	2.278(1)/2.280(1)
	N−O	1.129(1.145)	1.140(2)/1.141(2)

[a]Values in parentheses are computed on the free cations (optimized without PF_6^-).

tendency for a slightly inflated coordination sphere in the computed structures is observed, with largest differences of 0.047 and 0.056 Å observed for the $Ru-N_{py}$ distances in the free $[RuCl(NO)py_4]^{2+}$ and $[RuCl(ON)py_4]^{2+}$cations, respectively. This effect has previously been observed in ruthenium complexes[51] and may tentatively be assigned to the influence of the solid state environment. Furthermore, these differences are reduced to 0.037 and 0.049 Å in $[RuCl(NO)py_4]^{2+}$ and $[RuCl(ON)py_4]^{2+}$, respectively, if the PF_6^- anions are introduced in the computation (Table 8).

In addition, the computations ran in the presence of PF_6^- anions lead to the observation of longer Ru−NO (1.779 vs 1.770 Å) and Ru−ON (1.925 vs 1.887 Å) computed bond lengths in the presence of PF_6^-. This suggests that the counterions play a role in the capability for isomerization observed in the solid state.

Computed Gibbs free energies ($\Delta G°$) carried out on the ruthenium complexes with and without PF_6^- counterions are reported in Table 9 for $[RuCl(NO)py_4]^{2+}$ and $[RuCl(ON)py_4]^{2+}$. Data indicate always that the ground state conformation is $[RuCl(NO)py_4]^{2+}$.

Table 9. Influence of the Counteranion on the DFT-Computed Energetic Gap between the Isonitrosyl Conformation of the MS1 State and the Ground State Nitrosyl Conformation of $[RuCl(NO)py_4]^{2+}$

complex	Counteranions	$\Delta G_{GS} - \Delta G_{MS1}$ (kcal·mol^{-1})
$[RuCl(NO)py_4]^{2+}$	none	39.1
	PF_6^-	34.4

We would like to point out that the presence of anions leads to a stabilization of the $[RuCl(ON)py_4]^{2+}$ metastable isomer with respect to the situation encountered in the free cation (39.1 and 34.4 kcal·mol^{-1} for the free cation and the PF_6^- salt, respectively). This effect likely arises from the observation that the interactions with the anions are less pronounced in Ru−NO than in Ru−ON (computed Ru−NO···F short contact of 2.63 Å reduced to 2.41 Å in Ru−ON···F in qualitative agreement with the X-ray values of 2.910 and 2.886 Å in Ru−NO···F and Ru−ON···F, respectively). From differential scanning calorimetry 24.8 kcal/mol is received[34] for the decay of MS1 in the PF_6 compound, which deviates by about 17% from the calculated data.

This study suggests that the energetic properties of the linkage isomers are largely influenced by the environment, which is consistent with the intuition that the formally +1 charged nitrosyl ligand may strongly interact with the anions during its rotation in the solid state as also pointed out in an earlier study on $Ru(NH_3)_5NO$ compounds.[52] Observation of the shift of the H_2O vibrational bands to lower energies in MS2 and higher energies in MS1, where different hydrogen bonds of O···H (GS) and N···H (MS1) are formed, indicates the influence of the environment. Furthermore, while it is possible to stabilize a metastable linkage (MS2) isomer with side-on configuration by DFT in the free complex cation, the presence and nature of the anions may lead to decoordination of NO during the computational process in this configuration. This unexpected result suggests that the energy barrier is also significantly reduced in the Ru−NO to Ru−ON crossover process. Altogether, these calculations support the idea that in the solid state the anion plays an important role in the photoswitching process.

Equatorial Ligand Influence. Pyridine ligands are substituted by 2,2′-bipyridine and 2,2′:6′,2″-terpyridine ligands in $[RuCl(NO)bpy_2](PF_6)_2$ (**8**) and $[RuCl_2(NO)tpy](PF_6)$ (**9**), respectively.

The influence of the ligands in the cis position with respect to the nitrosyl is as important as that of the ligands in trans position. Earlier studies performed on the series of *trans*-hydroxynitrosylruthenium $[Ru(OH)(NO)L_4]^{n+}$ (L_4 = $(bpy)_2$, $(NH_3)_4$) complexes evidence the ligand effect on the NO vibration frequency.[36,53] However, there is no direct relationship between the nature of the ligands in the cis position and the population of the metastable states or their decay temperature.

Complexes $[RuCl(NO)py_4](PF_6)_2·1/2H_2O$ (**1**) and $[RuCl(NO)bpy_2](PF_6)_2$ (**8**) exhibit two types of equatorial ligands which are comparable in terms of electronic nature, except for the delocalization on the bipyridines. Moreover, they contain identical counterions and the same ligand in the trans position to NO. While the pyridine ligands of **1** have a high degree of freedom as they can freely rotate for adopting a more stable conformation, the bipyridine ligands of **8** are rigid because of the C−C bond connecting pyridine cycles constraining them to a planar configuration. This higher degree of freedom of the pyridine ligand might explain that the conversion yields are 5 times higher in $[RuCl(NO)py_4](PF_6)_2·1/2H_2O$ (**1**) than in **8**. During the NO rotation the pyridine rings can freely rotate, and in the metastable configuration they can adapt to the novel configuration to lower the overall energy. In contrast the bipyridine ligands are severely restrained in their flexibility, and this seems to be unfavorable for achieving high populations.

Table 10. ν_{NO} Downshift and Populations of the MS1 Metastable State in $[RuCl_2(NO)tpy]^+$ and $[RuCl(NO)bpy_2]^{2+}$ versus $[RuCl(NO)py_4]^{2+}$

compounds	ν_{GS} (cm^{-1})	ν_{MS1} (cm^{-1})	ν_{NO} downshift (cm^{-1})	P_{MS1} (%)
$[RuCl(NO)py_4](PF_6)_2·1/2H_2O$ (**1**)	1911	1777	134	76
$[RuCl(NO)bpy_2](PF_6)_2$ (**8**)	1928	1810	118	15
$[RuCl_2(NO)tpy](PF_6)$ (**9**)	1896−1914−1925	1776−1788	120−137	8

dx.doi.org/10.1021/ic202702r | Inorg. Chem. 2012, 51, 7492−7501

Complex $[RuCl_2(NO)tpy](PF_6)$ (**9**) shows a slightly different structure from the reference complex (**1**). In **9**, one of the nitrogen atoms of the terpyridine ligand is in the position trans to NO while the other two nitrogen atoms occupy two of the equatorial ligand positions. Furthermore, two chlorine atoms complete the equatorial plane. This combination of the rigid terpyridine ligand and the two chlorine atoms leads to a MS1 population in **9**, which is about 10 times lower than in **1** (Table 10).

Trans Ligand of NO Influence. Complexes of **1** and **5**, **2** and **6**, as well as **3** and **7** are compared in pairs in order to analyze the influence of the trans ligand of NO on the population. In the three cases, the trans ligand Cl (**1**, **2**, or **3**) is substituted by Br (**5**, **6**, or **7**) while the counteranion is unaltered PF_6^-, BF_4^-, or Br^-, respectively (Table 11).

Table 11. Influence of the Nature of the Trans Ligand of NO on the Photochromic Response[a]

complexes	trans ligand of NO	P_{MS1} (%)	donor effect of the trans ligands of NO on the metastable state population
$[RuCl(NO)py_4](PF_6)_2 \cdot 1/2H_2O$ (**1**)	Cl	76	decrease of 40%[b]
$[RuBr(NO)py_4](PF_6)_2$ (**5**)	Br	46	
$[RuCl(NO)py_4](BF_4)_2 \cdot 1/2H_2O$ (**2**)	Cl	45	decrease of 38%[b]
$[RuBr(NO)py_4](BF_4)_2$ (**6**)	Br	28	
$[RuCl(NO)py_4]Br_2 \cdot 3/2H_2O$ (**3**)	Cl	17	decrease of 70%[b]
$[RuBr(NO)py_4]Br_2$ (**7**)	Br	5	
$[RuCl(NO)bpy_2](PF_6)_2$ (**8**)	Cl	15	decrease of 21%[c]
$[Ru(H_2O)(NO)bpy_2](PF_6)_3$ (**10**)	H_2O	19	

[a]The donating ability of the used ligands is H_2O < Cl < Br. [b]$(P_{MS1}(Cl) - P_{MS1}(Br))/P_{MS1}(Cl)$. [c]$(P_{MS1}(H_2O) - P_{MS1}(Cl))/P_{MS1}(H_2O)$.

Although complexes **1** and **5** crystallize in different space groups, their crystal structures evidence two intermolecular contacts between PF_6^- and the NO ligand. In **1** and **5**, the 40% decrease of the population seems to originate from the change of the ligand in trans to NO. Similar results are obtained by comparing complexes **3** and **7** (70% decrease of the MS1 population) and complexes **2** and **6** (38% decrease of the MS1 population). In order to confirm this observation, we compared the MS1 population of two bipyridine complexes. From $[Ru(H_2O)(NO)bpy_2](PF_6)_3$ (**10**) to $[RuCl(NO)bpy_2](PF_6)_2$ (**8**) the population decreases by 21%, one-half of the change observed for complexes with pyridine ligands.

The donating ability of the used ligands is as H_2O < Cl < Br. In the four conducted comparisons (**1** and **5**, **2** and **6**, **3** and **7**, and **8** and **10**), the population of the MS1 state decreases when the donating character of the ligand in trans to NO increases. Moreover, studies on the $[RuX(NO)(en)_2]^{n+}$ (X = Cl, Br, H_2O) and $[RuX(NO)(NH_3)_4]^{n+}$ (X = NH_3, OH, H_2O)[36] series show the increase of the MS1 decay temperature when the donating character of the X ligand in the trans position to NO decreases. This result confirms that metastable states are favored when weak donating ligands are trans to NO.

CONCLUSION

We studied a series of ruthenium mononitrosyl complexes based on *trans*-$[RuX(NO)py_4]^{2+}$ cations with X = Cl and Br in order to rationalize the parameters that favor the photochromic response, which is of importance with respect to potential applications. Using single-crystal X-ray diffraction the structures of five compounds were determined revealing the presence of intermolecular contacts between the counterions and the nitrosyl ligand which favor the photoswitching efficiency. The IR study of complexes **1**–**6** shows that the nature of the counteranion affects the photochromic property of the ruthenium cation. The population of metastable states can be amplified by a factor of 7 from 11% to 76% in powdered samples when the counterion Cl^- is substituted by PF_6^-. DFT calculations and infrared spectroscopy evidence the importance of direct intermolecular contacts between the NO ligand and the counteranions. The Jahn–Teller-induced rotation of the N–O ligand is not suppressed by the short contacts due to the local change of the electron density in the $Ru-N_{NO}$ bond. This is in agreement with the existence of both isomers in crystals with different kind of phase transitions[54] so that the driving force for formation of the isomers is located in the M–N–O bonds. However, the efficiency (population) depends on the external influence (contacts) as shown in this article.

We also investigated the influence of the nature of the equatorial ligands and the ligand trans to NO on the photoconversion. Complexes **8** and **9** show a drastic decrease of the conversion yield related to the rigidity of the bipyridyl and terpyridyl ligands compared to the more flexible pyridine ligands. The donating effect of the ligand in trans position from NO has also consequences on the photocommutation, as observed in the study of complexes **1**–**5**, **2**–**6**, **3**–**7**, and **8**–**10**.

All of these interactions are responsible for the shift of the energy minimum and reaction coordinate (as defined in Scheme 2) for GS and MS. This leads to an increase or decrease of the absorption cross sections for the population σ_{pop} and depopulation σ_{depop} at the same wavelength. While for **1** the ratio is $\sigma_{pop}/\sigma_{depop} \gg 1$, in all other cases the potential shift reduces σ_{pop} or increases σ_{depop} such that the achievable population decreases. Therefore, central atoms, ligands, and counterions can tune the population via their influence on the energy surface, which can be seen in the ratio of $\sigma_{pop}/\sigma_{depop}$.

In conclusion, this work brings out the particular influence of the nature of the counterion on the photochromic properties of mononitrosyl cationic ruthenium complexes. It would now be interesting to extend this study to other mononitrosyl complexes in order to identify other structural effects which enhance the photochromic response.

ASSOCIATED CONTENT

Supporting Information

CIF files for **2**, **3**, **4**, **5**, and **9**; IR spectra for **3**–**5** and **8**–**10**; DFT-computed structures for $[RuCl(NO)py_4](PF_6)_2$, $[RuCl(NO)py_4]^{2+}$, $[RuCl(ON)py_4](PF_6)_2$, and $[RuCl(ON)py_4]^{2+}$. This material is available free of charge via the Internet at http://pubs.acs.org.

AUTHOR INFORMATION

Corresponding Author

*E-mail: isabelle.malfant@lcc-toulouse.fr.

Notes

The authors declare no competing financial interest.

REFERENCES

(1) Grenthe, I.; Nordin, E. *Inorg. Chem.* **1979**, *18*, 1109–1116.
(2) Decurtins, S.; Gutlich, P.; Köhler, C. P.; Spiering, H.; Hauser, A. *Chem. Phys. Lett.* **1984**, *105*, 1–4.
(3) Gutlich, P.; Garcia, Y.; Woike, T. *Coord. Chem. Rev.* **2001**, *219–221*, 839–879.

(4) Goujon, A.; Varret, F.; Escax, V.; Bleuzen, A.; Verdaguer, M. *Polyhedron* **2001**, *20*, 1339−1345.
(5) Coppens, P.; Novozhilova, I.; Kovalevsky, A. *Chem. Rev.* **2002**, *102*, 861−884.
(6) Kovalevsky, A. Y.; Bagley, K. A.; Coppens, P. *J. Am. Chem. Soc.* **2002**, *124*, 9241−9248.
(7) Sato, O. *Acc. Chem. Res.* **2003**, *36* (9), 692−700.
(8) Yam, V. W.-W.; Ko, C.-C.; Zhu, N. *J. Am. Chem. Soc.* **2004**, *126*, 12734−12735.
(9) Dorbes, S.; Valade, L.; Réal, J. A.; Faulmann, C. *Chem. Commun.* **2005**, 69−71.
(10) Kume, S.; Nishihara, H. *Dalton Trans.* **2008**, *25*, 3260−3271.
(11) Woike, T.; Kirchner, W.; Shetter, G.; Barthel, T.; Hyung-sang, K.; Haussühl, S. *Opt. Commun.* **1994**, *106*, 6−10. Günter, P.; Huignard, J. P. *Photorefractive materials and their application*; Springer: Berlin, 1988.
(12) Ashley, J.; Bernal, M.-P.; Burr, G. W.; Coufal, H.; Guenther, H.; Hoffnagle, J. A.; Jefferson, C. M.; Marcus, B.; Macfarlane, R. M.; Shelby, R. M.; Sincerbox, G. T. *IBM J. Res. Dev.* **2000**, *44*, 341−368.
(13) Kawata, S.; Kawata, Y. *Chem. Rev.* **2000**, *100*, 1777−1788.
(14) Rose, M. J.; Mascharak, P. K. *Coord. Chem. Rev.* **2008**, *252*, 2093−2114. Fry, N. L.; Mascharak, P. K. *Acc. Chem. Res.* **2011**, *44*, 289−298. Schatzschneider, U. *Eur. J. Inorg. Chem.* **2010**, 1451−1467. Ford, P. C.; Wecksler, S. *Coord. Chem. Rev.* **2005**, *249*, 1382−1395. Bordini, J.; Ford, P. C.; Tfouni, E. *Chem. Commun.* **2005**, *33*, 4169−4171.
(15) Goulkov, M.; Schaniel, D.; Woike, T. *J. Opt. Soc. Am. B* **2010**, *27*, 927−932.
(16) Hauser, U.; Oestriech, V.; Rohrweck, H. D. *Z. Phys. A* **1977**, *280*, 17−25.
(17) Hauser, U.; Oestriech, V.; Rohrweck, H. D. *Z. Phys. A* **1977**, *280*, 125−130.
(18) Woike, T.; Zöllner, H.; Krasser, W.; Haussühl, S. *Solid State Commun.* **1990**, *73*, 149−152.
(19) Woike, T.; Haussühl, S. *Solid State Commun.* **1993**, *86*, 333−337.
(20) Guida, J. A.; Piro, O. E.; Aymonino, P. J. *Inorg. Chem.* **1995**, *43*, 4113−4116.
(21) Fomitchev, D. V.; Coppens, P.; Li, T.; Bagley, K. A.; Chen, L.; Richter-Addo, G. B. *Chem. Commun.* **1999**, *19*, 2013−2014.
(22) Da Silva, S. C.; Franco, D. W. *Spectrochim. Acta, Part A* **1999**, *55A*, 1515−1525.
(23) Schaniel, D.; Woike, T.; Boskovic, C.; Gudel, H. U. *Chem. Phys. Lett.* **2004**, *390*, 347−351.
(24) Schaniel, D.; Woike, Th.; Biner, D.; Kraemer, K.; Guedel, H. U. *Phys. Chem. Chem. Phys.* **2007**, *9*, 5149−5157.
(25) Bitterwolf, T. E. *Inorg. Chem. Commun.* **2008**, *11*, 772−773.
(26) Schaniel, D.; Woike, Th.; Behrnd, N. R.; Hauser, J.; Kraemer, K.; Todorova, T.; Delley, B. *Inorg. Chem.* **2009**, *48*, 11399−11406.
(27) Carducci, M. D.; Pressprich, M. R.; Coppens, P. *J. Am. Chem. Soc.* **1997**, *119*, 2669−2678.
(28) Schaniel, D.; Woike, T.; Schefer, J.; Petricek, V. *Phys. Rev. B: Condens. Matter Mater. Phys.* **2005**, *71*, 174112−1−174112−7.
(29) Cormary, B.; Malfant, I.; Buron-Le Cointe, M.; Toupet, L.; Delley, B.; Schaniel, D.; Mockus, N.; Woike, T.; Fejfarova, K.; Petricek, V.; Dusek, M. *Acta Crystallogr., Sect. B* **2009**, *65*, 612−623.
(30) Schaniel, D.; Woike, T. *Phys. Chem. Chem. Phys.* **2009**, *11*, 4391−4395.
(31) Atanasov, M.; Schönherr, T. *J. Mol. Struct. (THEOCHEM.)* **2002**, *592*, 79−93.
(32) Corronado, E.; Klokishner, S.; Reu, O.; Tsukerblat, B. *Adv. Quantum Chem.* **2003**, *44*, 429−444.
(33) Schaniel, D.; Nicoul, M.; Woike, T. *Phys. Chem. Chem. Phys.* **2010**, *12*, 9029−9033.
(34) Schaniel, D.; Cormary, B.; Malfant, I.; Valade, L.; Woike, T.; Delley, B.; Kraemer, K. W.; Guedel, H.-U. *Phys. Chem. Chem. Phys.* **2007**, *9*, 3717−3724.
(35) Schaniel, D.; Schefer, J.; Delley, B.; Imlau, M.; Woike, T. *Phys. Rev. B: Condens. Matter Mater. Phys.* **2002**, *66*, 085103−1−085103−10.
(36) Schaniel, D.; Woike, T.; Delley, B.; Boskovic, C.; Biner, D.; Kraemer, K. W.; Guedel, H.-U. *Phys. Chem. Chem. Phys.* **2005**, *7*, 1164−1170.
(37) (a) Nagao, H.; Nishimura, H.; Funato, H.; Ichikawa, Y.; Howell, F. S.; Mukaida, M.; Kakihana, H. *Inorg. Chem.* **1989**, *28*, 3955−3959. (b) Adeyemi, A.; Miller, F.; Meyer, T. J. *Inorg. Chem.* **1972**, *11*, 994−999.
(38) Ferlay, S.; Schmalle, H. W.; Francese, G.; Stoeckli-Evans, H.; Imlau, M.; Schaniel, D.; Woike, T. *Inorg. Chem.* **2004**, *43*, 3500−3506.
(39) Sheldrick, G. M. *SHELXL-97, Program for Crystal Structure Refinement*; University of Göttingen: Göttingen, 1997. Farrugia, L. J. ORTEP3 for Windows. *J. Appl. Crystallogr.* 1997, *30*, 565−568.
(40) Frisch, M. J.; Trucks, G. W.; Schlegel, H. B.; Scuseria, G. E.; Robb, M. A.; Cheeseman, J. R.; Scalmani, G.; Barone, V.; Mennucci, B.; Petersson, G. A.; Nakatsuji, H.; Caricato, M.; Li, X.; Hratchian, H. P.; Izmaylov, A. F.; Bloino, J.; Zheng, G.; Sonnenberg, J. L.; Hada, M.; Ehara, M.; Toyota, K.; Fukuda, R.; Hasegawa, J.; Ishida, M.; Nakajima, T.; Honda, Y.; Kitao, O.; Nakai, H.; Vreven, T.; Montgomery, Jr., J. A.; Peralta, J. E.; Ogliaro, F.; Bearpark, M.; Heyd, J. J.; Brothers, E.; Kudin, K. N.; Staroverov, V. N.; Kobayashi, R.; Normand, J.; Raghavachari, K.; Rendell, A.; Burant, J. C.; Iyengar, S. S.; Tomasi, J.; Cossi, M.; Rega, N.; Millam, J. M.; Klene, M.; Knox, J. E.; Cross, J. B.; Bakken, V.; Adamo, C.; Jaramillo, J.; Gomperts, R.; Stratmann, R. E.; Yazyev, O.; Austin, A. J.; Cammi, R.; Pomelli, C.; Ochterski, J. W.; Martin, R. L.; Morokuma, K.; Zakrzewski, V. G.; Voth, G. A.; Salvador, P.; Dannenberg, J. J.; Dapprich, S.; Daniels, A. D.; Farkas, O.; Foresman, J. B.; Ortiz, J. V.; Cioslowski, J.; and Fox, D. J. *Gaussian 09*, Revision A.02; Gaussian, Inc.: Wallingford, CT, 2009.
(41) Becke, A. D. *J. Chem. Phys.* **1993**, *98*, 564−573.
(42) Lee, C.; Yang, W.; Parr, R. G. *Phys. Rev. B* **1988**, *37*, 785−789.
(43) Hay, P. J.; Wadt, W. R. *J. Chem. Phys.* **1985**, *82*, 270−283.
(44) Guida, J. A.; Piro, O. E.; Aymonino, P. J. *Solid State Commun.* **1986**, *57*, 175−178.
(45) Guida, J. A.; Ramos, M. A.; Piro, O. E.; Aymonino, P. J. *J. Mol. Struct.* **2002**, *609*, 39−46.
(46) Ookubo, K.; Morioka, Y.; Tomizawa, H.; Miki, E. *J. Mol. Struct.* **1996**, *379*, 241−247.
(47) Kushch, L. A.; Golhen, S.; Cador, O.; Yagubskii, E. B.; Il'in, M. A.; Schaniel, D.; Woike, T.; Ouahab, L. *J. Cluster Sci.* **2006**, *17*, 303−315.
(48) Kawano, M.; Ishikawa, A.; Morioka, Y.; Tomizawa, H.; Miki, E.-i.; Ohashi, Y. *Dalton Trans.* **2000**, *14*, 2425−2431.
(49) Morioka, Y.; Ishikawa, A.; Tomizawa, H.; Miki, E.-i. *Dalton Trans.* **2000**, *5*, 781−786.
(50) Cormary, B. Université Paul Sabatier, Toulouse, 2009.
(51) Labat, L.; Lamère, J. F.; Sasaki, I.; Lacroix, P. G.; Vendier, L.; Asselberghs, I.; Pérez-Moreno, J.; Clays, K. *Eur. J. Inorg. Chem.* **2006**, *15*, 3105−3113.
(52) Schaniel, D.; Woike, Th.; Kushch; Yagubskii, E. *Chem. Phys.* **2007**, *340*, 211−216.
(53) Togano, T.; Kuroda, H.; Nagao, H.; Maekawa, M.; Nishimura, H.; Howell, F. S.; Mukaida, M. *Inorg. Chim. Acta* **1992**, *196*, 57−63.
(54) Zöllner, H.; Krasser, W.; Woike, Th.; Haussühl, S. *Chem. Phys. Lett.* **1989**, *161*, 497−501.